V International Conference on Particle-based Methods – Fundamentals and Applications
PARTICLES 2017
P. Wriggers, M. Bischoff, E. Oñate, D.R.J. Owen, & T. Zohdi (Eds)

DEM ANALYSIS OF EFFECT OF INTERFACIAL TRANSITIONAL ZONES ON FRACTURE IN CONCRETE

MICHAŁ NITKA AND JACEK TEJCHMAN

Faculty of Civil and Environmental Engineering
Gdańsk University of Technology
Narutowicza 11/20, 80-233, Gdańsk, Poland
micnitka@pg.gda.pl, tejchmk@pg.gda.pl

Key words: DEM, concrete, 3D, ITZ, 3-point bending beam.

Abstract. The aim of this paper is to show 3D numerical results on progressive fracture of the concrete at aggregate level using discrete element method (DEM). The test were performed for three point bending beam. Concrete was modelled as heterogeneous material consisted four phases: aggregate, cement matrix, interfacial transitional zones (ITZs) and air voids. The microstructure of sample as position and shapes of aggregate and air voids were taken directly from laboratory test. The non-destructive method of X-ray microCT scans was used. The numerical results (both macro- and microscopic) were directly compared with own laboratory test and previous 2D calculations. The special attention was lied on the crack geometry evolution. The effect of different properties of ITZ was studied.

1 INTRODUCTION

Fracture of the concrete materials strongly depends upon a heterogeneous structure of materials over many different length scales. It is a fundamental and complex phenomenon in quasi brittle materials [1-3]. To better understand its behaviour the meso-scale level should be accurate described in numerical analysis. The concrete sample may be described as a four-phase material composed of aggregate, cement matrix, macro-voids and interfacial transitional zones. The presence of aggregate and ITZs is particularly important since the volume fraction of aggregate can be as high as 70-75% in concrete. The calculation outcomes in [4,5] evidently showed that considering real size and shape of aggregate was essential. Also the ITZ phase should be modelled since it is always the weakest regions in usual concretes wherein micro-cracking starts [6]. The highly heterogeneous ITZ are attractors for a crack propagation. ITZs are porous regions of the cement paste around aggregate particles which are perturbed by their presence. Its thickness is about 5-50 μm. Their origin lies in the packing of the cement grains against the much larger aggregate that leads to a local increase in porosity (micro-voids) and a presence of small cement particles. A paste with the lower *w/c* (higher packing density) or made of finer cement particles or smooth aggregates lead to ITZs of a smaller extent. (higher packing density) or made of finer cement particles or smooth aggregates lead to ITZs of a smaller extent. These layers are highly heterogeneous and damaged and thus critical for the concrete behaviour. The accurate understanding of the properties and behaviour of ITZ is one of the most important issues in meso-scale analyses because damage is initiated in the weakest region and ITZs are

just the weakest link in concrete.

The meso-modelling can be used to comprehensively study local phenomena at the micro-level such as the mechanism of the initiation, growth and formation of localized zones and cracks which affect the macroscopic concrete behaviour. In this paper the discrete element method was chosen as a good tool to describe fracture [2,4,5,7-16]. A non-linear response of concrete during bending under 3D conditions was analysed. The calculations were performed with the 3-dimensional open-source code YADE which was developed at Grenoble University [17,18]. A linear contact under compression was used. The normal and tangential contact forces satisfied the cohesive-frictional Mohr-Coulomb equation [12]. The internal structure of concrete (size, shape and location of aggregate and macro-voids, micro-porosity) was directly taken from 3D x-ray images using the micro-tomography SkyScan 117 [4,5]. The numerical results were compared with previous 2D calculations and with laboratory test [4]. The special attention was laid on the crack path and on influence of the ITZs properties.

2 OWN LABORATORY TEST ON CONCRETE BENDING BEAM

The notched concrete beam was used in experiments, with height H=80 mm, width B=40 mm and length L=320 mm. Notch was located in the middle and its height and width was equal 8 mm and 3 mm (Fig.1). The concrete mixture was composed of aggregate and sand grains ($d_{\max}$=16 mm, d_{50}=2 mm), Portland cement (CEM I 32.5 R) and water (the compressive strength was about 50 MPa). The total particle (aggregate and sand) volumetric content was V=75%. The total aggregate content with the diameter equal to or larger than 2 mm was V=37%. The initial porosity of concrete was about 5%. The concrete sample was subjected to quasi-static three-point bending test. The vertical force F_{max} was equal to 2.15 kN (the flexural tensile strength was $f_{t,flex}$=3.73 MPa). The more details about experiment can be found in [4,19].

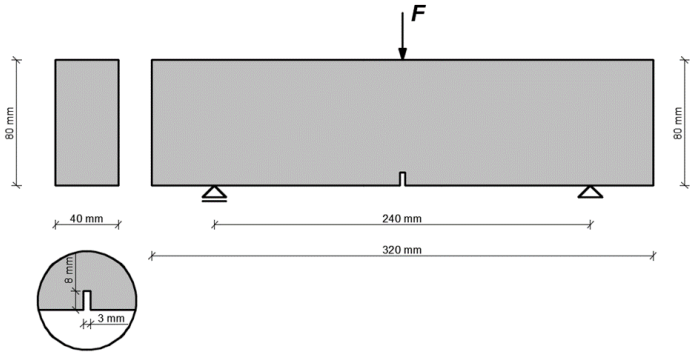

Fig.1: Geometry and boundary conditions of concrete beams subjected to three-point bending [4]

The distribution of aggregate and macro-voids in the concrete beams was determined based on microCT images of concrete cuboids (80×50×40 mm^3) cut from the middle part of beam after the tests [4]. Figure 2A shows 3D images of concrete internal structure obtained with the aid of SkyScan 1173 which represents a new generation in high-resolution desktop X-ray micro-computed tomography systems [19].

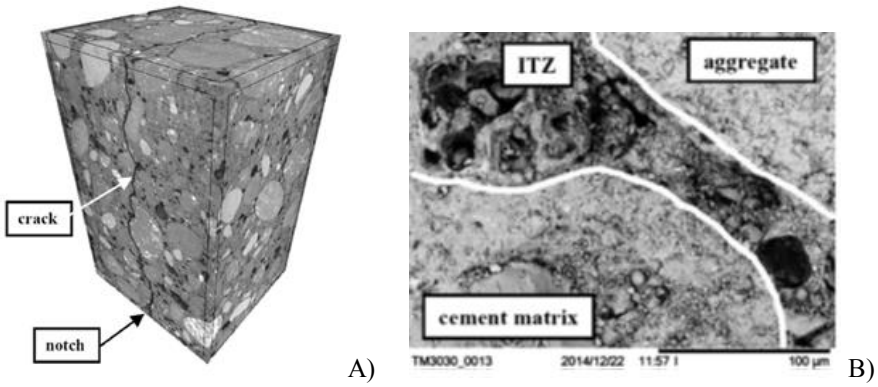

Fig.2: Experimental results: A) X-ray μCT images of cracked cuboidal specimens 80×50×40 mm^3 cut out from beam and B) scanning electron micrographs of ITZs around aggregate particles (magnification factor 1000) [4], [19]

The mine crack was strongly curved along beam height and width due to a random presence of aggregate grains and air voids (Fig.2A). It starts just above the notch and propagated upwards due to bending. The crack solely propagated through the weakest phase in concrete which were interfacial transitional zones (ITZs). Sometimes the crack can also propagate through a weak aggregate particle. Thus micro-cracking occurred first in ITZs and when two interfacial cracks occurred around adjacent aggregates, a crack inside the cement matrix initiated to bridge the interfacial cracks so that a connected crack path was formed. In order to observe porous structure of ITZs and measure its width, the scanning electron microscope (SEM) Hitachi TM3030 was used. The maximum magnification factor was 30'000. The width of ITZ varied between 30-50 μm and it did not depend on aggregate particle diameter (Fig. 2B) [4]. ITZs appeared around all aggregate grains (d_a≥2 mm) and usually covered about 80-90% of the aggregate circumference that was probably caused by a formation of water lenses beneath aggregate grains during mixing [23]. Other our experimental results showed that the width of ITZ reduced with decreasing aggregate roughness [5].

3 DISCRETE ELEMENT METHOD MODEL

The numerical analysis was performed by discrete element method (DEM). The open-source code YADE, developed at University of Grenoble, was used [17,18]. The code was successfully used for describing the behaviour of different engineering materials with a granular structure (mainly of granular materials by taking shear localization into account [20-23]). This model show also its capabilities in concrete fracture calculations under bending (2D analyses) [4] and uniaxial compression (2D and 3D simulations) [5,12]. Main advantage is ability to explicitly handle the discrete/heterogeneous nature of the material by modelling particle-scale properties including size and shape which play an important role in concrete fracture [4,5].

The algorithm used in the presented paper is based on the classical discrete element method formulation described by Cundall and Strack [24]. First, based on constitutive laws, interaction forces were calculated, when elements slightly interpenetrate each other. Next, the Newton's second law was used to compute acceleration of each particle, which was then time integrated to find the new position. This process was repeated until the simulation was finished.

The model takes advantage of the so-called soft-particle approach (i.e. the model allows for particle deformation which is modelled as an overlap of particles). During the simulations, particles may overlap that can be interpreted as a local contact deformation. A linear normal contact model under compression was used. The normal force was not restricted in compression. The interaction force vector representing the action between two spherical discrete elements in contact was decomposed into a normal and tangential vector, respectively. The normal forces acting on spheres were modelled by an elastic law with cohesion. The normal and tangential forces were linked to the displacements through the normal stiffness K_n and the tangential stiffness K_s (Fig.3) [17]

$$\vec{F}_n = K_n U \vec{N}, \tag{1}$$

$$\vec{F}_s = \vec{F}_{s,prev} + K_s \Delta \vec{X}_s . \tag{2}$$

where U is the overlap between spheres, $\vec{N}$ denotes the normal vector at the contact point, $\Delta\vec{X}$ is the increment of the relative tangential displacement and $\vec{F}_{s,prev}$ is the tangential force from the previous iteration. The stiffnesses were computed as the functions of the modulus of elasticity of the grain contact E_c and two neighbouring grain radii R_A and R_B (to determine the normal stiffness K_n) and the modulus of elasticity E_c and Poisson's ratio υ_c of the grain contact and two neighbouring grain radii R_A and R_B (to determine the tangential stiffness K_s), respectively [17]

$$K_n = E_c \frac{2R_A R_B}{R_A + R_B} \qquad \text{and} \qquad K_s = \nu_c E_c \frac{2R_A R_B}{R_A + R_B} . \tag{3}$$

If two grains in contact have the same size (R_A=R_B=R), the numerical stiffness parameters are equal to: K_n=E_cR and K_s=$\upsilon_c E_c$R, respectively (thus K_s/K_n=υ_c).

The contact forces $\vec{F}_s$ and $\vec{F}_n$ satisfied the cohesive-frictional Mohr-Coulomb equation (Fig.4d), used to capture the non-linear nature of concrete

$$\| \vec{F}_s \| - F^s_{\max} - \| \vec{F}_n \| \cdot \tan\mu \le 0 \quad \text{(before contact breakage)} \tag{4}$$

and

$$\| \vec{F}_s \| - \| \vec{F}_n \| \cdot \tan\mu \le 0 \quad \text{(after contact breakage)}, \tag{5}$$

where μ denotes the inter-particle friction angle and $\vec{F}^s_{\max}$ is the cohesive force between spheres. In tension, the maximum admissible normal force was $\vec{F}^n_{\min}$ if there was no a geometric contact between elements. If this normal force between spheres $\vec{F}^n_{\min}$ was reached, the contact was broken. Moreover, if any contacts between grains re-appeared, cohesion between them was not taken into account. A crack was considered as open if cohesive forces between grains (Eq.4) disappeared when a critical threshold was reached. The movement of fragments (mass-spring systems with cohesion) was similar to the rigid body movement.

A choice of a very simple constitutive law was intended to capture on average various contact possibilities in real concrete. Both the interparticle cohesive force and tensile force were

assumed as a function of the interparticle cohesive stress C (maximum shear stress at pressure equal to zero), interparticle tensile normal stress T and sphere radius R [17], [25]

$$F^{s}_{\max} = C \cdot R^2 \qquad \text{and} \qquad F^{n}_{\min} = T \cdot R^2 . \tag{6}$$

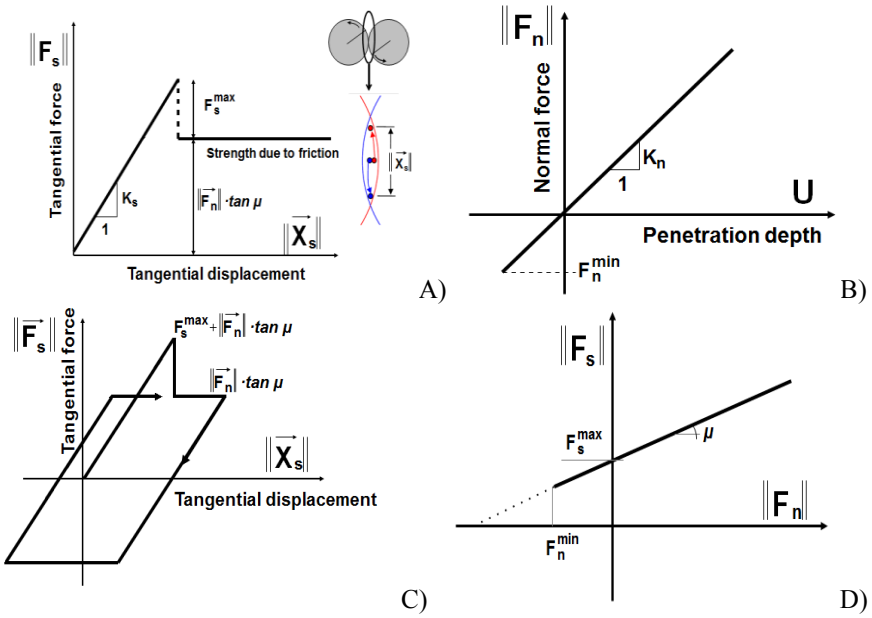

Fig.3: Mechanical response of DEM: A) tangential contact model, B) normal contact model, C) loading and unloading path in tangential contact model and D) modified Mohr-Coulomb model [12]

For two elements in contact, the smaller values of C, T and R were used. Because the proposed DEM is a fully dynamic formulation, a local non-viscous damping scheme was applied in order to dissipate excessive kinetic energy in a discrete system and facilitate convergence towards quasi-static equilibrium [26]. The damping parameter α_d was introduced to reduce contact forces acting on elements

$$\vec{F}^{k}_{damped} = \vec{F}^{k} - \alpha_d \cdot \mathrm{sgn}(\vec{v}^{k}) \,|\, \vec{F}^{k} \,|, \tag{7}$$

where $\vec{F}^{k}$ are the k[th]-components of the residual force and translational velocity, respectively. The positive damping coefficient α_d was smaller than 1 (sgn(•) returns the sign of the k[th] component of velocity). The equation could be separately applied to each k[th] component of the 3D vector x, y and z. The crack was not allowed to propagate through aggregate grains, i.e. the grain breakage has not been taken into account yet.

4 NUMERICAL ANALYSI

4.1 Input data

The concrete was modelled as four-phase material which consist aggregate cement matrix, ITZs and macro voids. The full 3D DEM analysis was performed on one concrete beam with exactly the same location and shapes of aggregate and macro voids as in experiment.

The specimen density (different phases) was determined with the aid of x-ray micro tomography. To describe the position of each voxel and its density (Figs.4Aa and 4Ba) the wave front *.obj file format was used. The high density shows aggregate (Fig.4Aa). The voxels with the density equal to the air density were assumed to be the macro-voids (Fig.4Ba). Next, the density volume was filled in with spheres (Figs.4Ab and 4Bb). The aggregate particles with the diameter higher than 2 mm were modelled only. The numerical volume of aggregate was 37% as in the experiment. All aggregate particles (2 mm$<d_a\leq$16 mm) were modelled as grain clusters with the diameter of d=2 mm (included from 2 up to 300 depending on its diameter) and all of them included ITZs around. ITZs were simply modelled as contacts between aggregate and cement matrix grains (thus they had no a physical width) in order to reduce calculations time. Note that simulation of the width of ITZs (0.03 mm - 0.05 mm) in the cement matrix would require very small spheres that would hugely increase the computational time. The spheres (0.5 mm$\leq d_{cm}<$2 mm) were solely assumed in the cement matrix; thus the smallest particle diameter in the specimen was 0.5 mm. The cement matrix grains filled the concrete specimen in about 97%. The macro-voids (with the diameter $d_{mv}\geq$1 mm) were modelled as empty regions.

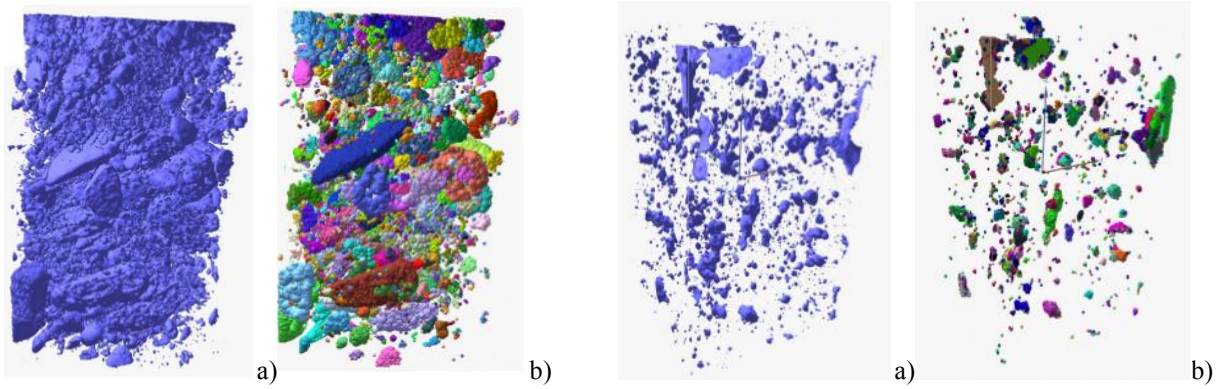

Fig.4: Three-dimensional view on aggregate (A) an macro-voids (B): a) based on density maps from x-ray micro tomographic images and b) replaced by elements (each colour corresponds to different diameter of aggregate cluster or macro-void)

The following five main local material parameters were needed for our discrete simulations: E, υ, μ, C and T. In addition, the particle radius R, particle mass density ρ and damping parameters α_d were required. Note that material softening was not assumed in the numerical model. The material parameters were calibrated in our previous 2D calculations [4]. The following parameters of the cohesion C and tensile strength T were used in all DEM analyses for the mid-region of the beam: cement matrix ($E_{c,cm}$=11.2 GPa, C_{cm}=140 MPa and T_{cm}=25 MPa) and ITZs ($E_{c,ITZ}$=7.8 GPa, C_{ITZ}=100 MPa and T_{ITZ}=17.5 MPa), which was 30% weaker than cement matrix. The choice of

reduction ratio was based on the experiments by nanoindentation [27]. With the assumed material properties and grain size distribution curve, the 2D and 3D DEM simulations provided the uniaxial compressive strength of about 50 MPa. similarly as in the experiments of Section 2 (f_c=51.81 MPa). In the remaining region outside the meso-region with large grains (Fig.5) was described by the same constants as form the cement matrix. The remaining parameters were constant for all phases and regions: υ_c=0.2 (Poisson's ratio of grain contact), μ=18^o (inter-particle friction angle), α_d=0.08 (damping parameter) and ρ=2.6 kG/m^3 (mass density). The prescribed damping parameter α_d and loading velocity v=2 mm/s did not affect the results (the inertial number I was <10^{-4} that always corresponded to a quasi-static regime) [12].

The beam with 3D particle clusters (Fig.5) included in total about 230'000 elements (220'000 elements in the meso-region 180'000 in the cement matrix and 40'000 in the aggregate) with d_{min}=0.5 mm. The calculations time was about 10-12 days using PC with CPU 3.30 GHz.

The detailed calibration procedure was described by [4,5,12] based on real laboratory tests on uniaxial compression or uniaxial tension of concrete specimens.

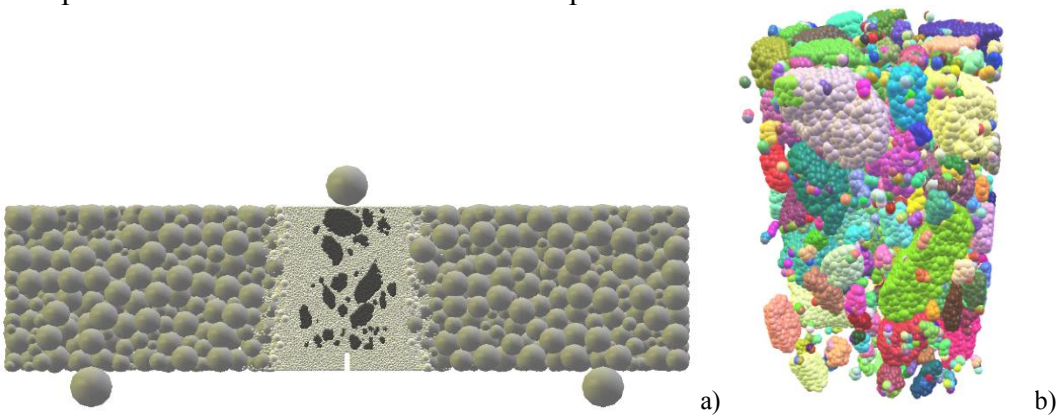

a) b)

Fig.5: Geometry of concrete beam model in DEM: a) front side of entire beam and c) 3D aggregate with ITZs in meso-region of 50×80×40 (each colour correspond different aggregate particles)

4.2 3D DEM results

The macroscopic numerical curves of vertical force versus CMOD were shown in Fig. 6. The 3D results were compared to previous 2D calculations and laboratory test. The obtained force peak (F=2.14 kN for CMOD=0.015 mm) was in good agreement with the experiment (F=2.18 kN for CMOD=0.017 mm). The residual force (CMOD=0.1 mm) was however higher by 100%. As compared to 2D results [4], the compressive strength was the same but the ductility was higher. Our earlier computations for uniaxial compression and tension [5,12] showed, the 3D calculations increase concrete ductility. The 3D curve was smoother than 2D curves due to a significantly larger number of particles in computations.

The crack path from 2D and 3D calculations and from laboratory test were presented in Fig. 7. The numerical crack shape in the vertical cross-section at the depth of 10 mm (Fig.7Ba) was like as in the experiment (Fig.7Aa). In the mid cross-section (Fig.7Bb) the shape was similar, however the aggregate just above notch was surround by crack from the other side than in the experiment (Fig.7Ab). Neverless both cracks ended at the same aggregate. In cross-section at the depth of 30 mm, the crack's onset had a different direction (Fig.7Ac) and furthermore the crack encircled next one aggregate grain along the opposite side, but finally ended at the same

position as the experimental macro-crack. As compared with 2D calculations [4], the calculated 3D crack path was similar (Figs.7Ca and 7Cc) or more realistic (see Fig.7Cb).

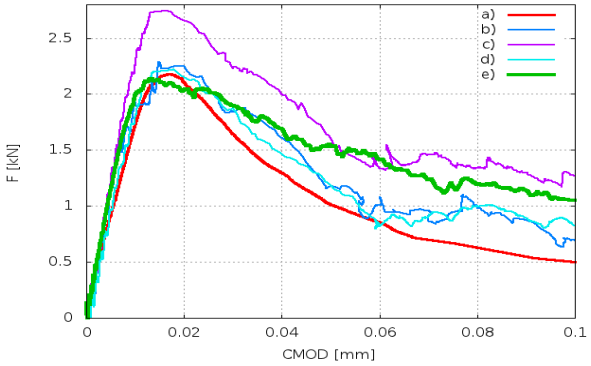

Fig.6: Evolution of vertical force *F* against CMOD in beam under 3-point bending: a) experimental curve (a), calculated curves in 3 different vertical cross-sections by 2D DEM (b-d) [4] and e) calculated curves by 3D DEM

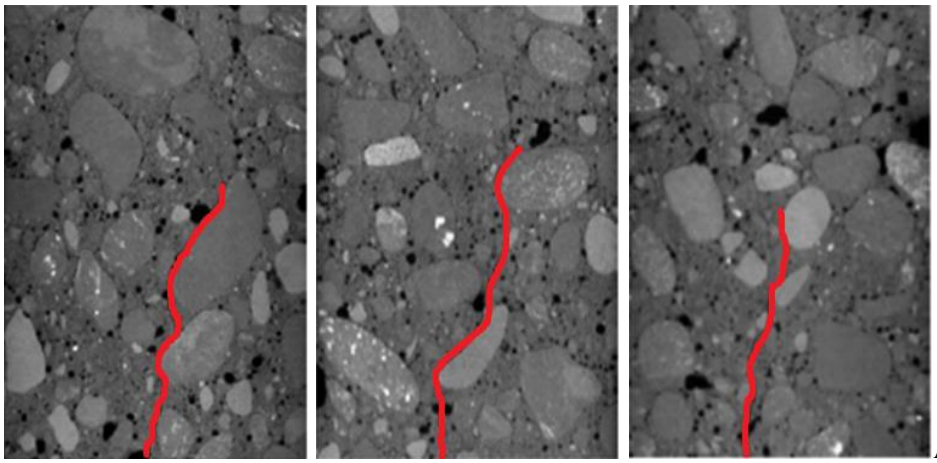
A)

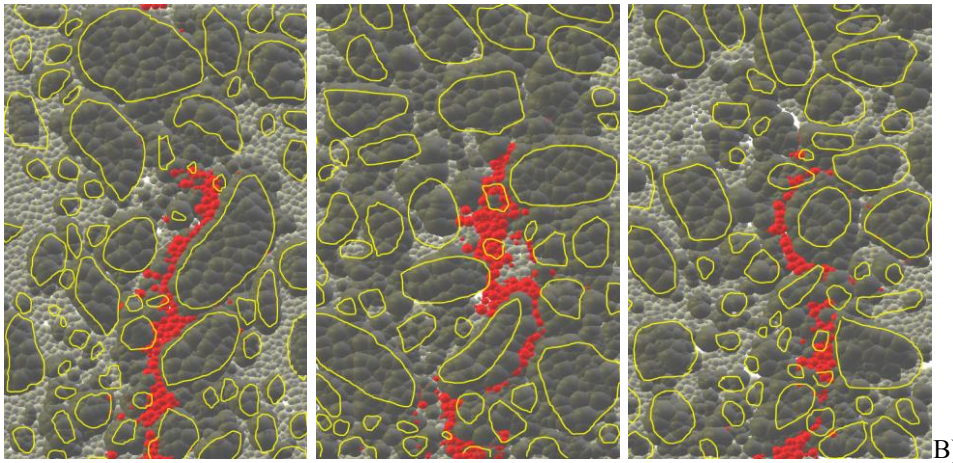
B)

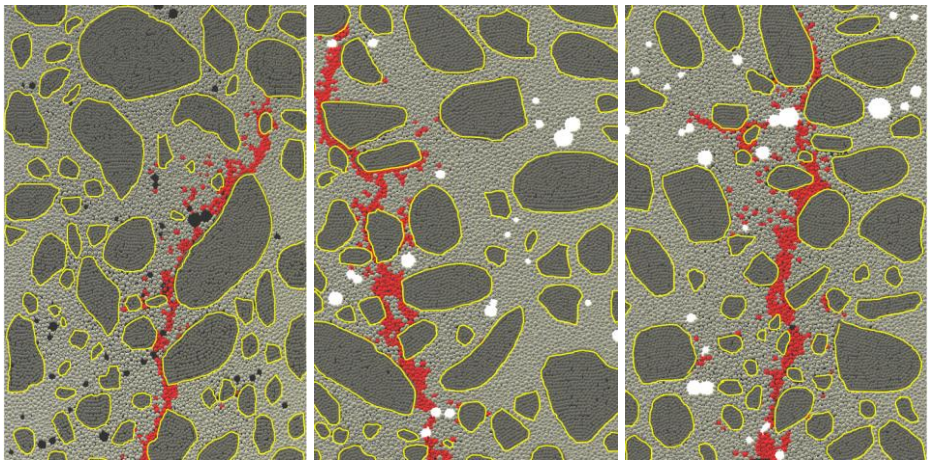
C)

Fig.7: Final crack trajectory in concrete beam above notch after test for CMOD=0.1 mm: A) based on micro-CT-image (red colour shows crack path), B) 3D DEM and C) 2D DEM [4] (red colour denotes elements with broken contacts, dark grey denotes aggregate, light grey denotes cement matrix) at depth of: a) 10 mm b) 20 mm and c) 30 mm from beam front side

4.3 Effect of ITZs properties

In Figure 8A the force – CMOD curves ware plotted for different strength of ITZs. The computations were performed for different ratios $E_{c,ITZ}/E_{c,cm}=C_{ITZ}/C_{cm}=T_{ITZ}/T_{cm}=r$ (with r=0.5, 0.7 and 0.9). The concrete beam stiffness and strength increase, since higher ratio was used (Fig. 8A). The material ductility increased with decreasing ratio r due to the growth of the macro-crack's propagation way through bridging interfacial micro-cracks. Thus, the macro-crack was more curved with the smaller ratio r (Fig.19B). For the ratio r=0.9, the macro-crack was almost straight. It propagated mostly through the cement matrix. For the ratio r=0.5, the macro-rack was more curved and propagated through the mortar and ITZs. The effect of r was similar in 3D and 2D analyses.

In Figure 9 the influence of the size of aggregates with ITZs was presented. Computations were done for ITZs phase around aggregate with diameter higher than 2mm (curve b) or higher than 3mm (curve c). The concrete strength, stiffness and brittleness became slightly higher with the smaller number of ITZ. The macro-crack's shape was not affected since the macro-crack was mostly attracted by ITZs located at large aggregate grains.

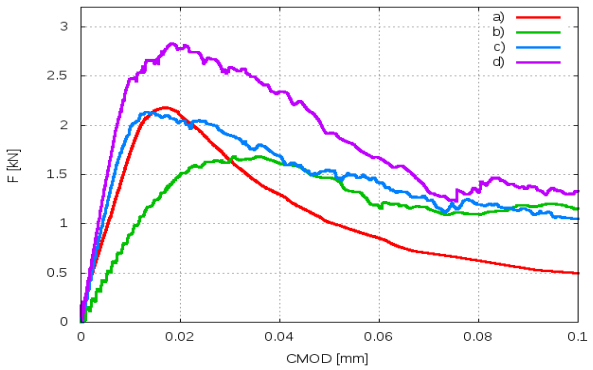

A)

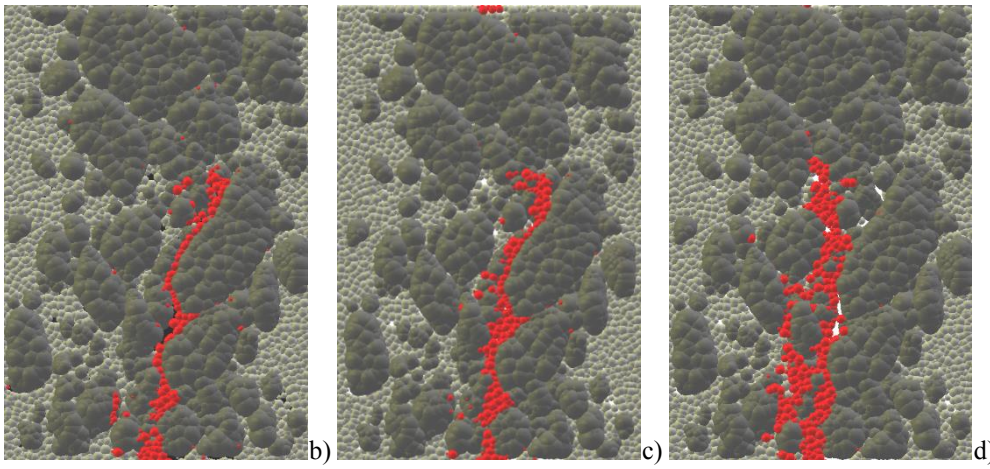

Fig.8: Effect of ITZs on evolution of vertical force F against CMOD (A) and crack shape (B) in beam under 3-point bending: a) experimental curve, b) $E_{c,ITZ}/E_{c,cm}$=0.5, C_{ITZ}/C_{cm}=0.5 and T_{ITZ}/T_{cm}=0.5, c) $E_{c,ITZ}/E_{c,cm}$=0.7, C_{ITZ}/C_{cm}=0.7 and T_{ITZ}/T_{cm}=0.7 and d) b) $E_{c,ITZ}/E_{c,cm}$=0.9, C_{ITZ}/C_{cm}=0.9 and T_{ITZ}/T_{cm}=0.9 (crack is shown in vertical cross-sectional slice at 10 mm from front specimen side for CMOD=0.1 mm)

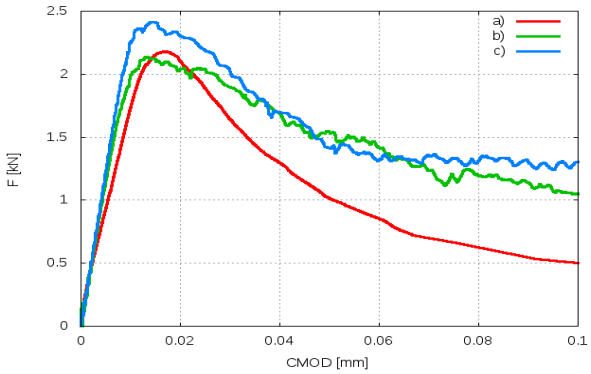

Fig.9: Effect of aggregate diameter with ITZs on evolution of vertical force F against CMOD in beam under 3-point bending: a) experimental curve, b) aggregate diameter d_a≥2 mm with ITZs and c) aggregate diameter d_a≥3 mm with ITZs

5 CONCLUSIONS

This paper shows capability of discrete element method (DEM) in fracture concrete calculations. The improvement between 2D and 3D calculations was presented. The 3D DEM model allow to understand micro-phenomena behaviour and predict the progressive nature of concrete fracture from the meso to macro level. Discrete models might progressively replace expensive experimental tests to study the influence of concrete meso-structure (aggregates size, aggregate shape, aggregate roughness, aggregate/mortar volume, micro- macro-porosity etc.) on the concrete behaviour. Thus the parametric studies within DEM might be used for the practical design of concrete with the improved desired performance. Directly from our numerical analysis, the following main conclusions may be pointed:

- The real shape of aggregate and the ITS around them have to be taken into calculations in order to realistic model micro fracture in concrete samples (i.e. bridging, branching).

- The influence of ITZs properties cannot be neglected in concrete modelling. With increasing stiffness and strength of this phase, the sample behave more brittle and its strength increase.
- The concrete strength, stiffness and brittleness became slightly higher with the smaller number of ITZs expressed by the larger diameter of aggregates d_a including ITZs.
- The shape and width of FPZ were more realistic since 3D calculations were performed. The macro response in force – CMOD curve was smoother, due to larger number of spheres in sample.

ACKNOWLEDGMENTS

The research work has been carried out within the project: ''*Innovative ways and effective methods of safety improvement and durability of buildings and transport infrastructure in the sustainable development*" financed partly by the European Union POIG.01.01.02-10-106/09-01) and the project ''*Experimental and numerical analysis of coupled deterministic-statistical size effect in brittle materials*" financed by the National Research Centre NCN (UMO-2013/09/B/ST8/03598).

REFERENCES

[1] Bažant, Z. and Planas, J. Fracture and size effect in concrete and other quasi-brittle materials. *CRC Press LLC*, Boca Raton (1997).
[2] Lilliu, G. and van Mier, J.G.M. 3D lattice type fracture model for concrete. *Engineering Fracture Mechanics* (2003) ***70***: 927-941.
[3] Tejchman, J. and Bobiński, J. Continuous and discontinuous modelling of fracture in concrete using FEM. *Springer, Berlin-Heidelberg (eds. W. Wu and R. I. Borja)* (2013).
[4] Skarżyński, Ł., Nitka, M. and Tejchman, J. Modelling of concrete fracture at aggregate level using FEM and DEM based on x-ray μCT images of internal structure, *Engineering Fracture Mechanics* (2015) **10** (147):13-35.
[5] Suchorzewski, J., Tejchman, J. and Nitka, M. Dicrete element method simulations of fracture in concrete under uniaxial compression based on its real internal structure, *International Journal of Damage Mechanics,* doi.: 10.1177/1056789517690915 (2017).
[6] Scrivener, K.L., Crumbie, A.K. and Laugesen, P. The interfacial transition zone (ITZ) between cement paste and aggregate in concrete. *Interface Science* (2004) **12**:411-421
[7] Du, C., Sun, L., Jiang, S. and Ying, Z. Numerical simulation of aggregate shapes of three-dimensional concrete and its applications. *Journal of Aerospace Engineer*ing (2013) 515-527.
[8] Hentz, S., Daudeville, L. and Donze, F. Identification and validation of a Discrete Element Model for concrete. *Journal of Engineering Mechanics ASCE* 130 (2004) **6**:709-719.
[9] Dupray, F., Malecot, Y., Daudeville, L. and Buzaud, E.A. Mesoscopic model for the behaviour of concrete under high confinement. *International Journal for Numerical and Analytical Methods in Geomechanics* (2009) **33:**1407-23.
[10] He, H., Guo, Z., Stroeven, P., Stroeven, M. and Sluys, L. J. Influence of particle packing on elastic properties of concrete. *Proc. First International Conference on Computational Technologies in Concrete Structures (CTCS'09),* Jeju, Korea, (2009), 1177-1197.
[11] Donzé, F.V., Magnier, S.A., Daudeville, L. and Mariotti, C. Numerical study of

compressive behaviour of concrete at high strain rates. *Journal for Engineering Mechanics,* 122(1999), **80:**1154-1163.
[12] Nitka, M. and J. Tejchman, J. Modelling of concrete behaviour in uniaxial compression and tension with DEM. *Granular Matter* (2015) **17,1**: 145-164.
[13] Groh, U., Konietzk, H., Walter, K. et al. Damage simulation of brittle heterogeneous materials at the grain size level, *Theoretical and Applied Fracture Mechanics* (2011) **55**:31-38.
[14] Carol, I., López, C.M., Roa, O. Micromechanical analysis of quasi-brittle materials using fracture-based interface elements. *International Journal for Numerical Methods in Engineering* (2001) **52**:193-215.
[15] Herrmann, H.J., Hansen, A. and Roux, S. Fracture of disordered, elastic lattices in two dimensions. *Physical Rev. B,* , (1989) **39**: 637-647.
[16] Kozicki, J. and Tejchman, J. Modelling of fracture processes in concrete using a novel lattice model. *Granular Matter* (2008) **10**, 377-388.
[17] Kozicki, J. and Donzé, F.V. A new open-source software developer for numerical simulations using discrete modeling methods. *Computer Methods in Applied Mechanics and Engineering* (2008) **197**:4429-4443.
[18] Šmilauer, V. and Chareyre, B. Yade DEM Formulation. Manual, (2011).
[19] Skarzynski, Ł. and Tejchman, J. Experimental investigations of fracture process in concrete by means of x-ray micro-computed tomography. *Strain* (2016) **52**:26-45.
[20] Widulinski, L., Tejchman, J., Kozicki, J. and Leśniewska, D. Discrete simulations of shear zone patterning in sand in earth pressure problems of a retaining wall. *Int. J. Solids and Structures* (2011) **48, 7-8**: 1191-1209.
[21] Kozicki, J., Niedostatkiewicz, M., Tejchman, J. and Mühlhaus, H.-B. Discrete modelling results of a direct shear test for granular materials versus FE results. *Granular Matter* (2013) **15, 5:** 607-627.
[22] Kozicki, J., Tejchman, J. and Műhlhaus, H.-B. Discrete simulations of a triaxial compression test for sand by DEM. *Int. J. Num. Anal. Methods Geom.* (2014) **38:** 1923-1952.
[23] Scrivener, K.L., Crumbie, A.K. and Laugesen, P. The interfacial transition zone (ITZ) between cement paste and aggregate in concrete. *Interface Science* (2004) **12:**411-421.
[24] Cundall, P.A. and Strack, O.D.L. A discrete numerical model for granular assemblies. *Geotechnique* (1979) **29**: 47-65.
[25] Ergenzinger, C., Seifried, R. and Eberhard, P.A. Discrete element model to describe failure of strong rock in uniaxial compression. *Granular Matter* (2011) **12(4):**341-364.
[26] Cundall, P.A. and Hart, R. Numerical modelling of discontinua. *Engineering Computations* (1992) **9:**101-113.
[27] Xiao, J., Li, W., Suc, Z., Lange, D.A. and Shah, S.P. Properties of interfacial transition zones in recycled aggregate concrete testes by nanoindentation, *Cement and Concrete Composites* (2013) **37:**276-292.